JPET#245050

Title page

HBT1, a novel AMPA receptor potentiator with lower agonistic effect, avoided bell-shaped response in *in vitro* BDNF production

Akiyoshi Kunugi, Yasukazu Tajima, Haruhiko Kuno, Satoshi Sogabe, and Haruhide Kimura

Research, Takeda Pharmaceutical Company Limited, Fujisawa, Kanagawa, Japan (A.K., Y.T., H.K., S.S., H.K.)

1

JPET#245050

Running title page

Running Title:

AMPA-R modulator with a lower risk of bell-shaped responses

Address correspondence to:

Haruhide Kimura, CNS Drug Discovery Unit, Research, Takeda Pharmaceutical Company

Limited, 26-1, Muraoka-higashi 2-chome, Fujisawa, Kanagawa 251-8555, Japan.

Phone number: (+81) 466321859

Fax number: (+81) 466294468

E-mail: haruhide.kimura@takeda.com

Number of text pages: 55

Number of figures: 8 (including three supplemental figures)

Number of tables: 3 in supplemental data

Number of references: 42

Number of words in Abstract: 243

Number of words in Introduction: 612

Number of words in Discussion: 1384

JPET#245050

Abbreviations:

AMPA, alpha-amino-3-hydroxy-5-methyl-4-isoxazole-propionic acid

AMPA-R, alpha-amino-3-hydroxy-5-methyl-4-isoxazole-propionic acid receptor

ATD, amino-terminal domain

BDNF, brain-derived neurotrophic factor

CHO, Chinese hamster ovary

CTZ, cyclothiazide

DMSO, dimethyl sulfoxide

EC_{50}, half maximal effective concentration

GluA1i CHO cells, GluA1i and TARPs γ2 expressing CHO cells

HBSS, Hanks' Balanced Salt Solutions

HBT1,

2-(((5-methyl-3-(trifluoromethyl)-1H-pyrazol-1-yl)acetyl)amino)-4,5,6,7-tetrahydro-1-benzot

hiophene-3-carboxamide

HEK, human embryonic kidney

His-ATD, His-tagged GluA2o ATD protein

His-LBD, His-tagged GluA2o LBD protein

His-MIF, His-tagged macrophage migration inhibitory factor protein

LBD, ligand-binding domain

3

JPET#245050

LDH, lactate dehydrogenase

MIF, macrophage migration inhibitory factor

OXP1,

(3S)-1-(4-tert-butylphenyl)-N-((1R)-2-(dimethylamino)-1-phenylethyl)-3-isobutyl-2-oxopyrro

lidine-3-carboxamide

SPA, scintillation proximity assay

Recommended section assignment:

Neuropharmacology

JPET#245050

Abstract

Alpha-amino-3-hydroxy-5-methyl-4-isoxazole-propionic acid (AMPA) receptor (AMPA-R)

potentiators with brain-derived neurotrophic factor (BDNF)-induction potential could be

promising as therapeutic drugs for neuropsychiatric and neurological disorders. However,

AMPA-R potentiators such as LY451646 have risks of narrow bell-shaped responses in

pharmacological effects, including *in vivo* BDNF induction. Interestingly, LY451646 and

LY451395, other AMPA-R potentiators, showed agonistic effects and exhibited bell-shaped

responses in the BDNF production in primary neurons. We hypothesized that the agonistic

property is related to the bell-shaped response and endeavored to discover novel AMPA-R

potentiators with lower agonistic effects. LY451395 showed an agonistic effect in primary

neurons, but not in a cell line expressing AMPA-Rs, in Ca^{2+} influx assays; thus, we used a

Ca^{2+} influx assay in primary neurons and, from a chemical library, discovered two AMPA-R

potentiators with lower agonistic effects:

2-(((5-methyl-3-(trifluoromethyl)-1H-pyrazol-1-yl)acetyl)amino)-4,5,6,7-tetrahydro-1-benzot

hiophene-3-carboxamide (HBT1) and

(3S)-1-(4-tert-butylphenyl)-N-((1R)-2-(dimethylamino)-1-phenylethyl)-3-isobutyl-2-oxopyrro

lidine-3-carboxamide (OXP1). In a patch-clamp study using primary neurons, HBT1 showed

little agonistic effect, while both LY451395 and OXP1 showed remarkable agonistic effects.

HBT1, but not OXP1, did not show remarkable bell-shaped response in BDNF production in

JPET#245050

primary neurons. HBT1 bound to the ligand-binding domain (LBD) of AMPA-R in a

glutamate-dependent manner. The mode of HBT1 and LY451395 binding to a pocket in the

LBD of AMPA-R differed: HBT1, but not LY451395, formed hydrogen bonds with S518 in

the LBD. OXP1 may bind to a cryptic binding pocket on AMPA-R. Lower agonistic profile

of HBT1 may associate with its lower risks of bell-shaped responses in BDNF production in

primary neurons.

Introduction

Accumulating lines of evidence are suggesting that dysfunction of glutamatergic signaling

contributes to cognitive deficits and mood disorder. The ionotropic glutamate receptor,

alpha-amino-3-hydroxy-5-methyl-4-isoxazole-propionic acid (AMPA) receptor (AMPA-R),

mediates the vast majority of fast excitatory neurotransmission in the central nervous system

(Kew and Kemp, 2005). AMPA-Rs are composed of four subunits (GluA1-4), which have flip

(i) and flop (o) splice isoforms, and native AMPA-Rs are most likely tetramers generated by

the assembly of one or more of these subunits (Boulter et al., 1990; Keinanen et al., 1990;

Nakanishi et al., 1990; Sommer et al., 1990; Fletcher et al., 1995). Adding to the complexity

of AMPA-Rs is RNA editing of a Q/R site of the GluA2, and also differential assembly with

auxiliary accessory transmembrane proteins such as transmembrane AMPA-R regulatory

proteins (TARPs) (Schoft et al., 2007; Kato et al., 2008; Tomita, 2010). The extracellular

portion of each AMPA-R subunit consists of two domains: a ligand-binding domain (LBD)

and an amino-terminal domain (ATD) (Sobolevsky et al., 2009). AMPA-R plays an important

role in synaptic plasticity, which is essential for learning and memory (Derkach et al., 2007).

In fact, AMPA-R potentiators improved cognitive performance in multiple tasks (O'Neill and

Dix, 2007; Shaffer et al., 2013). Importantly, some AMPA-R potentiators can induce

production of brain-derived neurotrophic factor (BDNF) and exhibit neurotrophic and

neuroprotective properties (Murray et al., 2003; O'Neill et al., 2004). As BDNF has been

considered to have a role in the pathophysiology of various neuropsychiatric disorders,

including depression (Balaratnasingam and Janca, 2012), AMPA-R potentiators with potential

to increase BDNF levels could be promising drugs to treat neuropsychiatric and neurological

disorders (O'Neill and Witkin, 2007).

AMPA-R agonists, which can activate all AMPA-Rs, including resting receptors, have

been shown to induce both desensitization of AMPA-R and seizure (Yamada, 1998; Beattie et

al., 2000; Ehlers, 2000). AMPA-R potentiators are considered to have better pharmacological

profiles because of their selective enhancement of physiological activation of AMPA-Rs in the

brain. However, AMPA-R potentiators such as LY451646, LY451395, and S18986 are

reported to elicit bell-shaped responses in various pharmacological effects: LY451646 is

reported to show bell-shaped responses in *in vivo* BDNF induction, and the bell-shaped

response of LY451395 in the radial maze task was described in the introduction section of a

report about LY451395 (Mackowiak et al., 2002; Bai et al., 2003; Fowler et al., 2004; Jhee et

al., 2006; Bernard et al., 2010). PF-4778574 is reported to have less than a 30-fold safety

margin against seizure in rodents (Shaffer et al., 2013). Thus, discovery of AMPA-R

potentiators with lower risks of these issues is needed.

In this study, we tried to understand the mechanisms of action underlying the bell-shaped

response of AMPA-R potentiators. We found that both LY451646 and LY451395 started to

exhibit a bell-shaped response at concentrations at which they started to show agonistic effect

in BDNF protein production in primary neurons. Thus, agonistic effect may be associated with the bell-shaped responses of AMPA-R potentiators. To gain more insight into this hypothesis, we conducted a high-throughput screening and discovered new AMPA-R potentiators with lower agonistic effect in Ca^{2+} influx assays in primary neurons, 2-((((5-methyl-3-(trifluoromethyl)-1H-pyrazol-1-yl)acetyl)amino)-4,5,6,7-tetrahydro-1-benzothiophene-3-carboxamide (HBT1) and (3S)-1-(4-tert-butylphenyl)-N-((1R)-2-(dimethylamino)-1-phenylethyl)-3-isobutyl-2-oxopyrrolidine-3-carboxamide (OXP1). Based on careful *in vitro* characterization of LY451395, HBT1, and OXP1 using binding assays, co-crystallization analysis, a patch-clamp study, Ca^{2+} influx assays, and BDNF assay, etc., here we provide evidence that agonistic effects of AMPA-R potentiators may be associated with their risks of bell-shaped responses in BDNF production in primary neurons. HBT1 is shown to be a novel AMPA-R potentiator with lower agonistic effects in Ca^{2+} influx assay, a patch-clamp study, and BDNF assay in primary neurons, and have a lower risk of bell-shaped responses in BDNF production in primary neurons.

9

JPET#245050

Materials and Methods

Chemicals.

2-(((5-methyl-3-(trifluoromethyl)-1H-pyrazol-1-yl)acetyl)amino)-4,5,6,7-tetrahydro-1-benzothiophene-3-carboxamide (HBT1),

(3S)-1-(4-tert-butylphenyl)-N-((1R)-2-(dimethylamino)-1-phenylethyl)-3-isobutyl-2-oxopyrrolidine-3-carboxamide (OXP1), LY451395, and LY451646 were synthesized by Takeda Pharmaceutical Company Limited. [^{3}H]-HBT1 and [^{3}H]-OXP1 were synthesized by Sekisui Medical Company Limited. S-AMPA was obtained from Enzo Life Sciences (Farmingdale, NY). NBQX was obtained from Wako (Tokyo, Japan) or Tocris (Bristol, UK). Cyclothiazide (CTZ) was purchased from Tocris. All other materials were obtained from standard commercial sources.

Animals. Sprague–Dawley rats were supplied by Charles River Laboratories Japan, Inc. (Yokohama, Japan). The animals were housed in a light-controlled room (12-h light/dark cycle, with lights on at 7:00 AM) and were habituated more than one week prior to experiments. The care and use of the animals and the experimental protocols used in this research were approved by the Experimental Animal Care and Use Committee of Takeda Pharmaceutical Company Limited.

JPET#245050

Preparation of rat primary neurons. Primary cultures of hippocampal neuronal cells were

prepared from fetal Sprague–Dawley rats at 19 days of gestation. Rat embryos were

decapitated and their whole brains were isolated. Hippocampi were dissected in ice-cold

Hanks' Balanced Salt Solutions (HBSS) under a microscope and then dispersed into cells

using a neural cell dispersion kit (Sumitomo Bakelite Co., Ltd., Tokyo, Japan). The

dissociated cells were suspended in Neurobasal medium containing B27 supplement (Thermo

Fisher Scientific Inc.), 2 mM L-glutamine (Lonza, Basel, Switzerland), 100 U/mL penicillin

(Lonza), 100 μg/mL streptomycin (Lonza), and 20 μg/mL gentamicin sulfate (Lonza). The

cells were plated on poly-D-lysine coated 96-well plates (Corning Incorporated) for Ca^{2+}

influx assay or poly-L-lysine coated 96-well plates (Sumitomo Bakelite) for other

experiments at a density of 5×10^4 cells/well and cultured in a humidified CO_2 incubator with

5% CO_2 at 37°C.

BDNF assay in primary neurons. After 5 days of culture, the cells were used for the BDNF

assay. Primary cultures of hippocampal neuronal cells were treated with compounds in the

presence or absence of AMPA (1 μM) and cultured in a humidified CO_2 incubator with 5%

CO_2 at 37°C for 24 h. The cells were washed once using phosphate buffered saline and were

collected using 60 μL of lysis buffer (20 mM Tris-HCl at pH 8.0, 137 mM NaCl, 10%

glycerol, 1% NP-40, 1% protease inhibitor cocktail [Sigma-Aldrich, St. Louis, MO]).

11

Concentrations of BDNF were measured using a BDNF Emax ImmunoAssay System

(Promega, Fitchburg, WI).

Lactate dehydrogenase (LDH) release assay using primary neurons. After 5 days of

culture, the cells were used for the LDH release assay. Primary cultures of hippocampal

neuronal cells were treated with compounds in the presence or absence of AMPA (1 μM) and

cultured in a humidified CO_2 incubator with 5% CO_2 at 37°C for 24 h. Concentrations of

LDH in the collected culture medium were measured using an LDH cytotoxicity detection kit

(Takara Bio Inc., Kusatsu, Japan). The amount of LDH release induced by the addition of

Triton X-100 (final 2%) was defined as the maximum releasable LDH activity (100%) in the

cells.

Whole-cell patch clamp recording using primary neurons. After 11-20 days of culture, the

cells were used for the whole-cell patch clamp recording. Whole-cell patch clamp technique

was used for recording current from cultured neurons of rat hippocampus. Patch electrodes

with tip resistances ranging from 3 to 5 MΩ were filled with an intracellular solution

containing (concentrations in mM) CsCl 135.0, $MgCl_2$ 1.0, HEPES 10.0, EGTA 10.0,

Mg-ATP 4.0, and Na_2-GTP 0.3, adjusted to pH7.3 with CsOH (osmolality 275-295 mosm/L).

The extracellular solution contained (concentrations in mM) NaCl 140.0, KCl 4.0, $CaCl_2$ 2.0,

12

JPET#245050

$MgCl_2$ 1.0, HEPES 10.0, $NaHCO_3$ 5.0, D(+)-glucose 10.0, TTX 0.001, and D-AP5 0.05,

adjusted to pH7.4 with NaOH (osmolality 300-315 mosm/L). All experiments were carried

out at room temperature and performed using an Axopatch 1B amplifier with pCLAMP 9

software or a MultiClamp 700B amplifier with pCLAMP 10 software (Molecular Devices,

LLC, Orleans Drive Sunnyvale, CA), low-pass filtered at 2 kHz, and stored on a computer

hard-disk for off-line analysis. Neurons were voltage-clamped at -80 mV. Steady-state inward

currents were evoked by the application of agonist and drug via Y-tube perfusion system. In

the absence of AMPA, an AMPA-R potentiator was applied for 60 s. In the presence of

AMPA, an AMPA-R potentiator was applied 20 s prior to 10-s AMPA stimulus. Data were

analyzed using Clampfit 9 or Clampfit 10 software (Molecular Devices). The current

magnitudes were calculated as the percentage of maximum current or percentage of agonist

control current.

Ca^{2+} influx assay using primary neurons. After 5 days of culture, the cells were used for the

Ca^{2+} influx assay. After removal of culture medium, 75 µL of fluorescent calcium indicator

dye solution (Calcium4 assay Kit, Dojindo, Kumamoto, Japan) in Ca^{2+} reaction buffer

(DMEM, 10 mM HEPES, and 0.05% BSA) containing 1.25 mM Probenecid (Dojindo) was

added and the cells were incubated for 60 min in 5% CO_2 at 37°C and washed once using 75

µL of fluorescent calcium indicator dye solution. After addition of 75 µL of fluorescent

13

calcium indicator dye solution to each well again, the relative increases in intracellular Ca^{2+}

levels induced by compounds in the presence and absence of 5 μM AMPA were monitored for

8.5 min using a fluorometric imaging plate reader. Activity of the compound was defined as

fluorescence intensity integrated over the entire period of measurement. Intensity of 0% was

defined as activity in the presence of only DMSO, while 100% was defined as activity in the

presence of 5 μM AMPA and 10 μM HBT1. EC_{50} values were calculated using logistic

regression analysis.

Transfected cell lines. Human AMPA-Rs (GluA1-4i and GluA1-4o), human TARPs γ2

cDNA, and kainate receptors (GluK1 and GluK2) were subcloned into pcDNA3.1(+) or

pcDNA3.1(-) Zeo mammalian expression vectors (Thermo Fisher Scientific Inc., Waltham,

MA). Each of the AMPA-Rs and TARPs γ2 expression vectors were co-introduced to Chinese

hamster ovary (CHO) cells using a Gene Pulser II Electroporation System (Bio-Rad

Laboratories, Inc., Hercules, CA). For kainate receptors, GluK1 or GluK2 expression vectors

were introduced to CHO cells alone. G-418 Sulfate (Wako) resistant clones were picked, and

one clone was selected finally using the Ca^{2+} influx assay.

Ca^{2+} influx assay using AMPA-Rs or GluK1/2 receptors expressing cell lines. CHO cells

co-expressing human AMPA-Rs (GluA1-4i and GluA1-4o) and human TARPs γ2 or CHO

14

JPET#245050

cells expressing kainate receptors (GluK1 and GluK2) were plated at 3×10^4 cells/well in a

96-well Black Clear plate (Corning Incorporated, Corning, NY) and incubated for 24 h in 5%

CO_2 at 37°C. After removal of the culture medium, 100 µL of fluorescent calcium indicator

dye solution (Calcium5 assay Kit, Molecular Devices, Inc., Sunnyvale, CA) in Ca^{2+} reaction

buffer (Hanks' Balanced Salt Solutions, 10 mM HEPES, and 0.1% BSA) containing 1.25 mM

Probenecid (Thermo Fisher Scientific Inc.) was added and the mixture was incubated for 60

min in 5% CO_2 at 37°C. After a 60–min incubation, the cells were washed once with 100

µL/well of Ca^{2+} reaction buffer and incubated with 100 µL/well of fluorescent calcium

indicator dye solution. This washing step was omitted in the experiments for evaluation of

subunit and splice-variant selectivity of compounds. Relative increases in intracellular Ca^{2+}

levels induced by the compounds in the presence and absence of 3 mM glutamate were

monitored for 3 min using a fluorometric imaging plate reader (CellLux, Perkin Elmer Life

and Analytical Sciences, Inc., Shelton, CT). For the GluK1/2 receptor assay, fluorescent

calcium indicator dye solution that included the compounds and dimethyl sulfoxide (DMSO;

defined as 0% activity) or 250 µg/mL Concanavalin A (defined as 100% activity) was used.

After a 60-min incubation, relative increases in intracellular Ca^{2+} levels induced by

compounds in the presence of 3 mM glutamate were monitored for 3 min using a fluorometric

imaging plate reader. Activity of compound was defined as the integrated value of

fluorescence intensities measured at all detection points. For the AMPA-Rs assay with 3 mM

15

glutamate, 0% was defined as activity in the presence of 3 mM glutamate and DMSO, while

100% was defined as activity in the presence of 3 mM glutamate and 300 μM CTZ or in the

presence of 3 mM glutamate and 10 μM LY451646. For the AMPA-Rs assay without

glutamate, 0% was defined as activity in the presence of only DMSO, while 100% was

defined as activity in the presence of 3 mM glutamate and 300 μM CTZ or in the presence of

3 mM glutamate and 10 μM LY451646. For the GluK1/2 assay, 0% was defined as activity in

the presence of 3 mM glutamate and DMSO, while 100% was defined as activity in the

presence of 3 mM glutamate and Concanavalin A. EC_{50} values were calculated using logistic

regression analysis.

Expression vector constructs for recombinant proteins. GluA2o LBD consists of residues

Asn413–Lys527 and Pro653–Ser796 of the full human GluA2o subunit with a GT linker

connecting Lys527 and Pro653. GluA2o cDNA was used as a template for PCR. Primer 1

(GCATATGCATCACCATCACCATCACACGACCGAAAACCTGTATTTTCAGGGATCCA

ATAAGACTGTTGTTGTCACCACA) and primer 2

(AAGATCCTCAGCACTTTCGATGGGGGGTACCCTTCTTGATCATGATAGATATCCC)

were used to generate the gene fragment S1 (which has an *Nde*I site and *Kpn*I site), and

primer 3

(GGGATATCTATCATGATCAAGAAGGGTACCCCCATCGAAAGTGCTGAGGATCTT)

and primer 4 (CGCGGCCGCTCAGCTGCCGCACTCTCCTTT) were used to generate the

gene fragment S2 (which has a *Kpn*I site and *Not*I site). The PCR products were subcloned

into pCR TOPO II vector. Plasmids were digested by *Nde*I/*Kpn*I for S1 and *Kpn*I/*Not*I for S2

and they were ligated and cloned into pRH8 vector (which is a pRSF-1b-derived vector with

an *Nde*I site inserted between the His6-tag region and the *Kpn*I site).

GluA2o ATD domain gene was obtained from the hGluA2o (22-404)-His / pcDNA3.3

vector, which contains a *TE*V cleavage site at both the N-terminus and C-terminus of GluA2

ATD consisting of residues Val22–Ser404 of the full human GluA2o subunit. The hGluA2o

(22-404)-His gene was generated through PCR amplification using GluA2o cDNA as a

template. Primer 1

(GATGGGTTGCGTAGCTGAAGGATCCGAAAACCTGTATTTTCAGGGTGTCTCTTCTA

ACAGCATACAG) and primer2

(ATAATAGCTAGCTTGGAAGTATAAATTCTCAGAAGGGAGCTCAGTAAGGGTAAC),

which have a *BamH*I / *EcoR*I site and *TE*V cleavage site, were used as PCR primers. This

plasmid was digested by *BamH*I / *EcoR*I and the obtained GluA2o ATD gene was cloned into

pSeqTag2 vector (Thermo Fisher Scientific Inc.) for addition of the human Igκ secretion

signal sequence.

Expression and purification of recombinant proteins. pRH8-GluA2-LBD plasmids were

17

transformed in *Escherichia coli* strain BL21 (DE3) cells, which were grown at 37°C to an

A600 of 0.6 to 0.8 in LB medium supplemented with antibiotics (kanamycin), prior to the

IPTG induction at a final concentration of 0.5 mM. Cultures were allowed to grow at 16°C for

20 h. The cells were then harvested by centrifugation and the GluA2-LBD was purified using

a Ni-NTA column (Qiagen, Hilden, Germany) in buffer containing 500 mM imidazole, 50

mM Tris-HCl, 150 mM sodium chloride, and 0.5 mM dithiothreitol, at pH 8.0. For the

scintillation proximity assay (SPA) binding assay, the protein was then purified by size

exclusion on a Superdex 200 column (GE Healthcare UK Ltd., Buckinghamshire, UK) in

buffer containing 20 mM HEPES, 50 mM sodium chloride, and 1 mM glutamate, at pH 7.0.

For crystallization trials, GluA2-LBD was purified using a Ni-NTA column, followed by

*TE*V-protease cleavage and additional Ni-affinity chromatography to remove the 6×His tag of

the N terminus. A final size exclusion step on a Superdex 200 column was employed to

remove small amounts of aggregate and residual contaminants. Glutamate (1 mM) was

provided as a supplement in all buffers throughout purification. After the last column, the

protein was concentrated to 10 to 15 mg/mL and stored in buffer containing 20 mM HEPES,

50 mM sodium chloride, and 1 mM glutamate, at pH 7.0.

pSeqTag2-GluA2–ATD plasmids were transfected to Freestyle 293 cells (Thermo Fisher

Scientific Inc.) and cultured for 3 days at 37°C in FreeStyle 293 Expression Medium (Thermo

Fisher Scientific Inc.). GluA2o ATD protein secreted into the culture medium was then

JPET#245050

harvested and purified on a Ni–NTA agarose column (Qiagen) in buffer containing 500 mM

imidazole, 50 mM Tris-HCl, 150 mM sodium chloride, and 0.5 mM dithiothreitol, at pH 8.0.

Subsequent *AcTE*V (Thermo Fisher Scientific Inc.) digestion and size exclusion

chromatography with Superdex 200 (GE Healthcare UK Ltd.) were carried out. After

filtration through the last column, the protein was concentrated to 1 to 2 mg/mL and stored in

buffer containing 20 mM Tris, 150 mM NaCl, and 1 mM DTT, at pH 7.5.

Scintillation proximity assay (SPA). First, 62.5 μg of YSi (2-5 μm) copper his-tag SPA

beads (PerkinElmer Inc., Waltham, MA) and 0.25 μg of His-tagged GluA2o LBD protein

(His-LBD) were incubated in 100 μL of PBS containing 0.01% NP-40 and the indicated

amount of glutamate in 96-well LumiNunc plates (Thermo Fisher Scientific Inc.) overnight at

4°C. Subsequently, test compound and tritium-labelled ligand (40 nM [^{3}H]-HBT1 or 100 nM

[^{3}H]-OXP1) were added to each well. For the SPA using His-tagged GluA2o ATD protein

(His-ATD), 62.5 μg of YSi (2–5 μm) copper his-tag SPA beads, and 0.25 μg of His-tagged

GluA2o ATD were incubated in 100 μL of PBS containing the indicated amount of glutamate

in 96-well LumiNunc plates for 1 h at room temperature. Subsequently, 100 nM [^{3}H]-OXP1

was added to each well. Specific binding was defined as total binding minus non-specific

binding, which was estimated in the presence of 0.25 μg of the control protein (His-tagged

macrophage migration inhibitory factor [MIF] protein) instead of His-LBD or His-ATD.

JPET#245050

Binding was initiated by addition of a radioligand and continued for 3–5 h at room

temperature. The radioactivity due to the amount of bound radioligand was measured using a

microplate scintillation counter (TopCount NXT, PerkinElmer Inc.). All compounds were

dissolved in DMSO and final concentration of solvent was kept to 3% DMSO for the

[^{3}H]-HBT1/LBD binding assay. EC$_{50}$ values were calculated using logistic regression

analysis.

Binding assay using rat hippocampal membrane. Adult male Sprague-Dawley rats at 6–8

weeks old were sacrificed. Their hippocampi were rapidly dissected, quickly frozen on solid

CO_2, and stored at –80°C until use. Frozen tissues were homogenized using a Polytron for 30

s in 3.4 volumes of ice-cold assay buffer (30 mM Tris-HCl at pH 7.4). The homogenate was

centrifuged at 20,000g for 20 min (4°C). The pellet was resuspended for 10 s in an equal

volume of assay buffer and centrifuged for 20 min. The homogenate was washed one more

time in an equal volume of assay buffer (for a total of three washes). Membranes were

resuspended in 3.4 volumes of assay buffer. The assay mixture consisted of 1.2 mg of

membrane protein, 90 nM [^{3}H]-HBT1, test compound, 0.025% NP-40, and assay buffer to a

final volume of 1.0 mL. Non-specific binding was determined with 10 μM LY451646. Assays

were performed in the presence of 3 mM glutamate except as indicated. Samples were

incubated at 37°C for 2 h and then were filtered through GF/B filters (GE Healthcare UK

20

Ltd.) presoaked in 0.03% polyethylenimine. Filters were washed with 20 mL of ice-cold assay buffer.

For the binding assay using [^{3}H]-AMPA, the mixture consisted of 0.3 mg of membrane protein, 4 nM [^{3}H]-AMPA, test compound, 50 mM KSCN, 0.01% NP-40, and assay buffer to a final volume of 1.0 mL. Non-specific binding was determined with 100 μM AMPA. Samples were incubated on ice for 1 h and then filtered through GF/B filters presoaked in 0.03% polyethylenimine. Filters were washed with 20 mL of ice-cold assay buffer.

The radioactivity retained on the filters was measured using a liquid scintillation counter (LSC-6100, ALOKA, Tokyo, Japan). Protein was determined following a bicinchoninic acid assay method (Thermo Fisher Scientific Inc.). All compounds were dissolved in DMSO and the final concentration of solvent was kept to less than 0.3% DMSO. EC_{50} values were calculated using logistic regression analysis.

X-ray crystallography of the GluA2o LBD/HBT1 complex and the GluA2o LBD/LY451395 complex. For crystallization trials, the compounds were added to a final concentration of 1.5 mM and incubated at 16°C for a few hours. Crystals were grown at 4°C using the vapor diffusion sitting-drop method, with drops containing a 1:1 (v/v) ratio of protein solution to reservoir solution. The reservoir solution contained 11–18% PEG 3350, 0.1 M sodium acetate, and 0.1 M zinc acetate, at pH 4.3–5.4. Prior to data collection, crystals

21

were immersed in mother liquor solution containing 30% glycerol and flash frozen in liquid

nitrogen. Diffraction data were collected from a single crystal at Advance Light Source Beam

Line 5.0.3 using a Quantum210 CCD detector (ADSC) and placed under a 100 K nitrogen

cryostream. Data sets were reduced and scaled using HKL2000 (Otwinowski and Minor,

1997). Structures were solved by molecular replacement using MOLREP (Vagin and

Teplyakov, 2010) from the CCP4 package (Winn et al., 2011) and the coordinates of the

GluA2-LBD associated with glutamate (PDB code 1FTJ) as a search model. The structures

were refined through an iterative procedure utilizing REFMAC (Murshudov et al., 2011)

followed by model building in COOT (Emsley et al., 2010). The dictionary files for the

ligands were prepared using AFITT (OpenEye Scientific Software, Cambridge, MA). The

final models were validated using Molprobity (Chen et al., 2010). Crystallographic processing

and refinement statistics are summarized in Supplemental Table 1. All structural figures were

generated using PyMOL (Schrödinger, LLC, New York, NY).

Statistical analysis. The statistical significance of the differences between the two groups

was assessed using Aspin-Welch's *t*-test or Student's *t*-test. Differences yielding P values

≤0.05 were considered significant. In the experiments that examined the effects of multiple

concentrations of test compounds, statistical significance was analyzed using Bartlett's test,

which was used for testing the homogeneity of variances, followed by one-tailed Williams'

JPET#245050

test (for parametric data, P>0.05 by Bartlett's test) or one-tailed Shirley-Williams test (for

non-parametric data, P≤0.05 by Bartlett's test) for comparing concentration-dependent effects

of multiple concentrations of test compounds with the control group. Differences yielding P

values ≤0.025 were considered significant. In the BDNF assay using AMPA, the statistical

significance of differences between control and LY451646, LY451395, or OXP1 was assessed

using Dunnett's test. Differences yielding P values ≤0.05 were considered significant.

Results

LY451646 and LY451395 showed a bell-shaped response for BDNF protein production in primary neurons. LY451646 (Fig. 1A) is reported to elicit a bell-shaped response for BDNF mRNA expression in rat hippocampus (Mackowiak et al., 2002). We examined the effect of LY451646 on BDNF production in primary neurons. AMPA concentration-dependently increased BDNF protein levels in primary neurons (Supplemental Fig. 1). Under the conditions, in agreement with the previous *in vivo* study, LY451646 triggered a bell-shaped response for BDNF protein production in primary neurons in the presence of low concentration of AMPA (1 μM corresponds to about 10% of maximal effective concentration of AMPA); the maximum effect of LY451646 on BNDF production was observed at 0.3 μM, but its effect was attenuated at higher concentrations (Fig. 1B). LY451395 (Fig. 1A), an AMPA-R potentiator with chemical structure similar to that of LY451646, also showed a bell-shaped response in the BDNF assay; the maximum effect of LY451395 on BNDF production was observed at 0.1 μM, but its effect was attenuated at higher concentrations (Fig. 1B). Interestingly, LY451646 and LY451395 showed agonistic effects and concentration-dependently increased BDNF protein levels at 0.3–3 μM and 0.1–1 μM, respectively, even in the absence of AMPA (Fig. 1B). Note that both LY451646 and LY451395 started to show bell-shaped response where they started to exhibit the agonistic effects. LY451646 at up to 1 μM showed little cytotoxicity in the presence and absence of

AMPA; LY451646 at 3 μM showed a weak cytotoxicity in the presence of AMPA, but not in

the absence of AMPA (Fig. 1C). LY451395 showed little cytotoxicity in the presence and

absence of AMPA (Fig. 1C). These results suggest that the cytotoxicity does not affect the

bell-shaped response. Since LY451646 and LY451395 had similar properties in the BDNF

assay, we used LY451395 for further *in vitro* characterization.

LY451395 had agonistic effects in primary neurons in patch-clamp and Ca^{2+} influx

assays. Since primary neurons were stimulated with LY451646 or LY451395 for a long

period (24 h) to measure BDNF protein production in primary neurons, the observed

agonist-like effects (BDNF production in the absence of AMPA) may not be related to their

intrinsic agonistic effects (Fig. 1B). For example, glutamate may be released from primary

neurons during 24 h culture. Thus, we conducted a patch-clamp study to examine whether

LY451395 has an intrinsic agonistic effect. LY451395 induced AMPA-R-mediated current

both in the presence and absence of agonist (AMPA) in primary neurons (Fig. 2A). Thus, we

hypothesized that the agonistic property is related to the bell-shaped response and endeavored

to discover novel AMPA-R potentiators with lower agonistic effects. However, the

patch-clamp study and the BDNF assay are not suitable for a screening assay, because they

are labor-intensive and low throughput. Thus, we further evaluated LY451395 by Ca^{2+} influx

assays using a cell line expressing AMPA-Rs or primary neurons. To our surprise, LY451395

induced Ca^{2+} influx both in the presence and absence of AMPA in primary neurons (Fig. 2B),

while LY451395 induced Ca^{2+} influx only in the presence of glutamate in GluA1i and TARPs

γ2 expressing CHO cells (GluA1i CHO cells) (Fig. 2C); the half maximal effective

concentration (EC_{50}) in the presence and absence of AMPA in primary neurons was 0.11 μM

and 0.88 μM, respectively, and EC_{50} in GluA1i CHO cells was 0.37 μM. Thus, the widely

used Ca^{2+} influx assays with cell lines expressing AMPA-Rs for drug screening may not be

suitable to discover AMPA-R potentiators with lower agonistic effects.

We next examined whether LY451395 binds to the glutamate-binding site on AMPA-R to

produce its agonistic effect. In a binding assay measuring the competitive inhibition of

[3H]-AMPA binding to rat hippocampal membranes, LY451395 did not inhibit [3H]-AMPA

binding to rat hippocampal membranes, while a competitive AMPA-R antagonist, NBQX, did

(Fig. 2D). Thus, LY451395 may allosterically activate AMPA-Rs in the absence of agonist in

primary neurons.

HBT1 activated AMPA-R in an agonist-dependent manner and increased BDNF protein

levels at a broader range of concentrations in primary neurons compared to LY451395

and OXP1. To discover novel AMPA-R potentiators with lower agonistic effect in primary

neurons, we initially screened the chemical library by a Ca^{2+} influx assay using GluA1i CHO

cells, and then characterized the agonistic effect of hit compounds for AMPA-R by a Ca^{2+}

influx assay using primary neurons. As a result, we discovered two unique AMPA-R

potentiators: HBT1 and OXP1 (Fig. 3A). Both HBT1 and OXP1 induced Ca^{2+} influx in a

glutamate-dependent manner in GluA1i CHO cells, with an EC_{50} of 4.6 μM and 2.5 μM,

respectively (Fig. 3, B and C), and their glutamate-dependent Ca^{2+} influx was suppressed by

NBQX (Fig. 3D). Both HBT1 and OXP1 induced Ca^{2+} influx in an AMPA-dependent manner

in primary neurons, with an EC_{50} of 1.3 μM and 4.3 μM, respectively (Fig. 3, E and F), and

their AMPA-dependent Ca^{2+} influx was suppressed by NBQX (Fig. 3G). Interestingly, HBT1

induced AMPA-R-mediated current only in the presence of AMPA in a patch-clamp study

using primary neurons, while OXP1 induced AMPA-R-mediated current both in the presence

and absence of AMPA (Fig. 3H). In a binding assay measuring the competitive inhibition of

[3H]-AMPA binding to rat hippocampal membranes, neither HBT1 nor OXP1 inhibited

[3H]-AMPA binding to rat hippocampal membranes (Supplemental Fig. 2). These results

suggest that OXP1 allosterically activates AMPA-Rs in the absence of agonist in primary

neurons. Next, we examined the effects of HBT1 and OXP1 on BDNF protein production in

primary neurons. HBT1 concentration-dependently increased BDNF protein levels in the

presence of AMPA, and the maximum effect of HBT1 was maintained at 1–10 μM. HBT1 at

up to 3 μM showed no increase of BDNF protein levels in the absence of AMPA (Fig. 3I).

OXP1 prompted a bell-shaped response in the presence of AMPA; the maximum effect of

OXP1 on BNDF production was observed at 1 μM, but its effect was attenuated at higher

concentrations (Fig. 3I). OXP1 at ≥ 1μM increased BDNF protein levels in the absence of

AMPA (Fig. 3I). Similar to LY451646 and LY451395, OXP1 started to exhibit the

bell-shaped response where it started to show agonistic effect in BDNF production in primary

neurons.

HBT1 showed no cytotoxicity in the presence or absence of AMPA, while OXP1 showed a

weak but significant cytotoxicity in the presence and absence of AMPA at 1–10 μM and

0.1–10 μM, respectively (Fig. 3J). Taken together, these results suggest that the lower

agonistic effect of HBT1 in the induction of both Ca^{2+} influx and AMPA-R-mediated current

may be associated with its lower risks of bell-shaped response in BDNF production in

primary neurons compared with LY451395 and OXP1.

Each subunit of AMPA-R has different function, and subunit selectivity of AMPA-R

potentiators may affect their functional outcomes (Ward et al., 2010). Thus, we examined the

subunit selectivity of HBT1 and OXP1 by Ca^{2+} influx assay using CHO cells expressing

GluA1-4i and TARPs γ2 or expressing GluA1-4o and TARPs γ2. As shown in Supplemental

Table 2, HBT1 and OXP1 showed little subunit selectivity. We also confirmed that these

compounds did not activate kainate receptors at concentrations up to 100 μM (Supplemental

Table 2).

To gain insight into the difference between these compounds, we investigated

concentrations of glutamate required for AMPA-R activation by HBT1 and OXP1 in GluA1i

CHO cells. Interestingly, HBT1 required higher concentration of glutamate than OXP1 to

activate AMPA-Rs; the EC_{50} of the glutamate concentration required to activate AMPA-R by

HBT1 and OXP1 was 2.5 μM and 0.25 μM, respectively (Fig. 3K), suggesting a difference in

modes of AMPA-R activation between HBT1 and OXP1.

HBT1 and LY451395 bound to a pocket in the LBD of AMPA-R with a different binding

mode. We examined the binding properties of HBT1 and OXP1 to AMPA-R. A hydrophilic

pocket at the dimer interface of the LBD of AMPA-R is known as a binding pocket for

several AMPA-R potentiators (Kaae et al., 2007; Sobolevsky et al., 2009). We investigated

the interaction between HBT1 and LBD using a SPA measuring the binding of radiolabelled

[3H]-HBT1 to a His-tagged GluA2o LBD protein (His-LBD). Specific interaction between

His-LBD and [3H]-HBT1 was detected in the presence of 100 μM glutamate; however, when

another His-tagged protein such as macrophage migration inhibitory factor (His-MIF) was

used instead of His-LBD, binding of [3H]-HBT1 was not detected. Thus, HBT1 may

specifically interact with Glu2o LBD (Fig. 4A). We also examined the interaction between

OXP1 and LBD using a SPA with [3H]-OXP1 and His-LBD. Specific interaction between

His-LBD and [3H]-OXP1 was not detected under our experimental conditions (Fig. 4B).

We next examined the effects of glutamate on the binding of [3H]-HBT1 to His-LBD.

Glutamate increased binding of [3H]-HBT1 to His-LBD in a concentration-dependent manner

(Fig. 4C). Thus, HBT1 would bind to LBD on AMPA-R in a glutamate-dependent manner.

The binding affinity of [^{3}H]-HBT1 to His-LBD was measured in the presence of 100 μM

glutamate. Analysis of the saturation isotherms gave a single saturable affinity binding site

(Kd = 543 nM) (Fig. 4D). In the SPA assay measuring the competitive inhibition of

[^{3}H]-HBT1 binding to His-LBD, HBT1 and LY451395 exhibited IC$_{50}$ of 0.64 μM and 0.03

μM, respectively (Fig. 4E).

The binding property of [^{3}H]-HBT1 to native AMPA-R was also assessed using rat

hippocampal membranes. Glutamate increased the binding of [^{3}H]-HBT1 to rat hippocampal

membranes in a concentration-dependent manner, and this [^{3}H]-HBT1 binding to rat

hippocampal membranes was not observed in the absence of glutamate (Fig. 4F). Analysis of

the saturation isotherms indicated a single saturable affinity binding site (Kd = 416 nM) (Fig.

4G). In the binding assay measuring the competitive inhibition of [^{3}H]-HBT1 binding to rat

hippocampal membranes, HBT1 and LY451395 exhibited an IC$_{50}$ of 0.28 μM and 0.02 μM,

respectively (Fig. 4H).

To understand the structural basis for the interaction between HBT1 and LBD, we

determined the crystal structures of the GluA2o LBD/glutamate/HBT1 complex and the

GluA2o LBD/glutamate/LY451395 complex. Data collection and refinement statistics are

shown in Supplemental Table 1. Both HBT1 and LY451395 bound to the cleft formed by the

dimer interface between the two protomers with a compound-to-protomer stoichiometry of

1:2 to stabilize the dimer interface in the active conformation (Fig. 4I). In the crystallographic

refinement, the dimer interface was occupied by two ligand molecules, which are related by a

noncrystallographic twofold axis, each with an occupancy of 0.5. Electron density maps of

HBT1 and LY451395 are shown in Supplemental Fig. 3.

We next examined the interaction of HBT1 and LY451395 with amino acid residues in the

LBD, using GluA2o LBD. For HBT1, the trifluoromethylpyrazole moiety and

tetrahydrobonzohiophene ring occupied two hydrophobic pockets of the dimer interface,

whereas two sulfonamide moieties of LY451395 occupied the same sites (Fig. 4J). The

hydrophobic pockets were composed of K514, P515, V771, and L772 in one protomer of the

dimer, and I502 and K751 in another protomer. The sulfonamide groups of LY451395 formed

hydrogen bonds with main-chain atoms of P515 and G752 in both pockets (Fig. 4J). HBT1

formed two hydrogen bonds with the side chain of S518 (Fig. 4J). The side chain of S518

exhibited two alternative conformations in the structure with HBT1, whereas S518 was found

in one conformation away from the compound to prevent steric clashes in the structure with

LY451395. Although LY451395 had no direct hydrogen bond with S518 or S750, the

biphenyl moiety made van der Waals contacts with P515 (Fig. 4J). HBT1 and LY451395 bind

to essentially the same site in the dimer interface with a distinct binding mode. The

sulfonamide groups of LY451395 made not only hydrophobic interactions, but also hydrogen

bonds with P515 and G752, whereas HBT1 occupied hydrophobic pockets without polar

31

interactions. This difference may be attributed to the lower binding potency of HBT1

compared with LY451395.

OXP1, via binding to a different site from that of HBT1, promoted binding between

HBT1 and AMPA-R and activated AMPA-R in the absence of agonist. We assessed

whether OXP1 affects the binding of [^{3}H]-HBT1 to the LBD by the two competitive binding

assays. Both in the SPA assay using His-LBD and in the binding assay using hippocampal

membranes, OXP1 failed to inhibit binding of [^{3}H]-HBT1 to His-LBD or hippocampal

membranes (Fig. 5, A and B). These data were in line with the data showing the lack of

binding between [^{3}H]-OXP1 and LBD (Fig. 4B). Considering that HBT1 and OXP1 had

similar potency in the Ca^{2+} influx assays (Supplemental Table 2, Fig. 3E and Fig. 3F), the

binding site of OXP1 on AMPA-R would differ from that of HBT1.

The AMPA-R ATD may possess an allosteric modulator site for small molecules, although

an AMPA-R ATD ligand has not been reported yet (Sukumaran et al., 2011). We investigated

the interaction between OXP1 and ATD by a SPA using [^{3}H]-OXP1 and a His-tagged

GluA2o ATD protein (His-ATD). Weak but specific-like interactions between His-ATD and

[^{3}H]-OXP1 were detected in the presence of 100 μM glutamate (Fig. 5C). When His-MIF was

used instead of His-ATD, no binding of [^{3}H]-OXP1 was detected (Fig. 5C). We examined the

effects of glutamate on the binding of [^{3}H]-OXP1 to His-ATD. Glutamate did not affect

JPET#245050

[3H]-OXP1 binding to His-ATD (Fig. 5D). To further investigate whether OXP1 activates

AMPA-R through the interaction with ATD, we introduced various point mutations in the

ATD of GluA2o by an alanine-scanning mutagenesis, and then mutant GluA2os were

expressed in human embryonic kidney (HEK) 293T cells. Evaluation of OXP1-induced Ca^{2+}

influx using HBT1 as a control LBD binder revealed that no GluA2o mutations selectively

reduced the activity of OXP1; GluA2o mutations that reduced the activity of OXP1 also

reduced the activity of HBT1 (Supplemental Table 3). More than 30 GluA2o mutations in the

ATD resulted in the reduction of the activity of HBT1 (< 20%), and these amino acids may be

critical to maintaining AMPA-R activity. Although we could not find the presumed OXP1

binding site in the ATD in this mutation study, there is still a possibility that OXP1 activates

AMPA-R through the interaction with those amino acid residues of the ATD.

AMPA-R potentiators discovered using a functional assay may have binding affinities to

multiple sites on AMPA-R, such as HBT1 binding site (HBT1-site) and OXP1 binding site

(OXP1-site). Thus, we examined the effects of HBT1-site and OXP1-site co-stimulation on

AMPA-R activation. As shown in Fig. 3 E and F, HBT1 and OXP1 did not induce Ca^{2+} influx

in the absence of AMPA in primary neurons at concentrations up to 30 and 10 μM,

respectively. Interestingly, co-application of 30 μM of HBT1 with 3 or 10 μM OXP1 induced

Ca^{2+} influx in the absence of AMPA in primary neurons (Fig. 5E), and that was not observed

in GluA1i CHO cells (Fig. 5F). The Ca^{2+} influx induced by the co-application of HBT1 with

JPET#245050

OXP1 (10 μM) was inhibited by NBQX (Fig. 5G). Co-stimulation with HBT1 and OXP1 may

activate AMPA-R in the absence of agonist in primary neurons. OXP1, but not HBT1, did

bind to AMPA-R in the absence of glutamate (Fig. 4F and Fig. 5D). Thus, we assessed

whether OXP1 can enhance binding of HBT1 to AMPA using [³H]-HBT1 and hippocampal

membranes in the absence of glutamate or in the presence of a low concentration of glutamate

(30 μM); we considered the possibility that co-stimulation with HBT1 and OXP1 can make

AMPA-R hypersensitive to a very low concentration of endogenous glutamate released from

primary neurons. OXP1 concentration-dependently increased the binding of [³H]-HBT1 to rat

hippocampal membranes under both conditions (Fig. 5H). Accordingly, OXP1 may enhance

binding of HBT1 to AMPA-R in the absence of agonist and in the presence of a low

concentration of agonist.

JPET#245050

Discussion

AMPA-R potentiators such as LY451646 and LY451395 have risks of narrow bell-shaped responses in various pharmacological effects, including *in vivo* BDNF induction (Mackowiak et al., 2002; Bai et al., 2003; Fowler et al., 2004; Jhee et al., 2006; Bernard et al., 2010). We found that LY451646 and LY451395 showed a bell-shaped response for BDNF protein production in primary neurons. Thus, the *in vitro* BDNF assay would be useful for the evaluation of risks of the bell-shaped response of AMPA-R potentiators, although further studies to investigate the relationship of those risks between the *in vitro* BDNF assay and *in vivo* pharmacological assays are needed.

LY451395 activated AMPA-Rs in the absence of an agonist in primary neurons in both the patch-clamp study and the Ca^{2+} influx assay, while it induced Ca^{2+} influx in a glutamate-dependent manner in a widely used GluA1i-expressing cell line. Thus, LY451395 seems to have agonistic effect against physiological AMPA-Rs. In line with this observation, LY404187, a racemic mixture that includes LY451646, was reported to induce large currents at concentrations higher than 1 μM during the recording (in the absence of agonist) in a patch-clamp study using primary neurons (Gates et al., 2001), while LY451646 was reported to show no intrinsic activity in cell lines expressing AMPA-Rs (Arai et al., 2000, Miu et al., 2001). The very low concentration of endogenous glutamate released from primary neurons would be related to this agonist-like effect of LY451395. Even so, LY451395 would be

35

JPET#245050

hypersensitive to glutamate and behave almost as an agonist in the brain. LY451395 showed

the agonistic effects in the patch-clamp study, the Ca^{2+} influx assay, and the BDNF assay,

from a concentration of around 0.3 μM, at which it started to show a bell-shaped response in

the presence of low concentration of AMPA in the BDNF assay. Thus, we hypothesized that

the agonistic effect was related to the bell-shaped response of AMPA-R potentiators. The

detailed mechanism of the bell-shaped response of LY451395 is unknown. Interestingly,

AMPA (pure agonist) did not show a bell-shaped response in the BDNF assay. Thus,

agonistic effect by AMPA and AMPA-R potentiators may have different impact on

AMPA-Rs and/or their downstream signal transduction machineries. Cells were stimulated

with compounds for a long period (24 h) in the BDNF assay, while cells were stimulated with

compounds for a short period both in the patch-clamp study (30 or 60 s) and the Ca^{2+} influx

assay (8.5 min). Due to this difference, the BDNF assay may have higher sensitivity to detect

the bell-shaped responses. Treatment of compounds for a long period might induce

desensitization of AMPA-R or its downstream signaling pathways, although further studies

are needed.

HBT1 and OXP1 had lower agonistic effects than LY451395 in Ca^{2+} influx assay using

primary neurons. In line with this result, HBT1 showed little agonistic effect in a patch-clamp

study using primary neurons. However, OXP1 showed remarkable agonistic effects in a

patch-clamp study using primary neurons. Binding site of OXP1 seemed to be different from

that of HBT1 and would not be located in the LBD. Thus, structural changes caused by OXP1

may differ from that by HBT1. This difference might contribute to difference in structure of

pore-forming domain and resulting Ca^{2+} permeability, although further studies would be

needed. AMPA-R-mediated BDNF production may depend on increase in intracellular Ca^{2+}

level (Hardingham et al., 1998; Tao et al., 1998; Shieh and Ghosh, 1999). Thus, BDNF

production in the absence of AMPA by OXP1 cannot be explained by its agonistic effect

observed in the patch-clamp study. OXP1 required lower concentration of glutamate to

activate AMPA-R compared with HBT1. Moreover, OXP1 can induce Ca^{2+} influx in the

presence of agonist. Thus, the very low concentration of endogenous glutamate released from

the excited primary neuron by OXP1-induced AMPA-R activation would be related to its

agonist-like effect in BDNF production. Further studies are needed to understand the detailed

mechanism of action of OXP1. Given that the patch-clamp study is labor-intensive with a low

throughput, both the Ca^{2+} influx assay and the patch-clamp study may be needed for the

screening of AMPA-R potentiators with lower agonistic effects.

Investigation of HBT1 and OXP1 binding sites revealed that HBT1, but not OXP1, bound

to the GluA2o LBD. From the X-ray crystallography analysis, HBT1, but not LY451395,

formed hydrogen bonds with S518 in the LBD; LY451395 formed hydrogen bonds with P515

and G752 in the LBD. Our results are consistent with the report that LY451646 interacted

with P515 and G752 in X-ray crystallography analysis (Kaae et al., 2007; Patel et al., 2013).

JPET#245050

Thus, amino acid residues used by HBT1 for interaction in the LBD would be different from those used by LY451395, and this difference may be associated with the lower agonistic effect of HBT1. It has been shown that glutamate binding changes the protein structure of the HBT1-site in the LBD (Armstrong and Gouaux, 2000; Yelshanskaya et al., 2014). [3H]-HBT1 bound to both His-LBD and rat hippocampal membrane only in the presence of glutamate. On the contrary, [3H]-LY395153, which is an arylpropylsulfonamide, is reported to modestly bind to rat cerebral cortical membranes in the absence of agonist (Zarrinmayeh et al., 2001). LY451395 may also bind to the LBD in the absence of agonist.

The AMPA-R ATD may possess an allosteric modulator site for small molecules, although no AMPA-R ATD ligand has been reported yet (Sukumaran et al., 2011). [3H]-OXP1 seemed to specifically bind to His-ATD in the SPA. This implies that the AMPA-R ATD may have a binding pocket for small molecules, and endogenous AMPA-R ATD ligand may also exist in the brain. However, [3H]-OXP1 had a low binding affinity to His-ATD, and the signal-to-noise ratio was about 2-fold in the SPA. Moreover, owing to lack of known ATD ligands, it is unclear whether the protein structure of His-ATD used in this study is close to that of physiological receptors. Further studies are needed to determine whether OXP1 really binds to the ATD. Since it is unknown whether the agonistic property is a common feature of OXP1-site binders, further assessment of compounds with binding affinity to OXP1-site may be worth trying.

To our surprise, co-stimulation with HBT1 and OXP1 activated AMPA-R in the absence of

agonists in primary neurons. AMPA-R activation by co-stimulation with HBT1 and OXP1,

LY451395 (Fig. 2C), or OXP1 (Fig. 3C) was not observed in GluA1i CHO cells in the

absence of glutamate. Therefore, a screening strategy depending on functional assays with

AMPA-R expressing artificial cell lines is insufficient, and understanding the binding site of

each chemotype is critical for discovery of AMPA-R potentiators with lower agonistic effects.

The protein structure of native AMPA-Rs is complicated; native AMPA-Rs are most likely

tetramers generated by the assembly of eight subunits (GluAi 1-4, GluAo 1-4) (Nakanishi et

al., 1990), and furthermore, the machinery responsible for assembly requires auxiliary

accessory transmembrane proteins such as TARPs (Tomita, 2010). Reconstruction of native

AMPA-R with these complexities may be difficult, and thus the properties of recombinant

AMPA-Rs in general would be critically different from those of native AMPA-R. In fact, a

Ca^{2+} influx assay using a cell line expressing recombinant AMPA-R could not detect

AMPA-R activation by glutamate (Miu et al., 2001). Therefore, functional assays using

primary neurons would be necessary to identify AMPA-R potentiators with lower agonistic

effect, although a screening assay using a large number of primary neurons is not realistic,

because it is labor-intensive and also lacks AMPA-R selectivity.

In summary, we have shown some evidence that agonistic effect may be associated with

bell-shaped response of AMPA-R potentiators. HBT1, a novel AMPA-R potentiator with

lower agonistic effects, had lower risks of bell-shaped response in *in vitro* BDNF production

compared with LY451646, LY451395, and OXP1. Unfortunately, HBT1 has a poor ADME

profile and is not suitable for *in vivo* studies. Discovery and development of novel AMPA-R

potentiators with lower agonistic effects like HBT1 may be worth considering. The screening

approach using the various binding and functional assays we show here (e.g., SPA using

[^{3}H]-HBT1 and His-LBD, X-ray crystallographic analysis, Ca^{2+} influx using cell lines

expressing AMPA-R and primary neurons, patch-clamp study using primary neurons, BDNF

assay) would be important to discover AMPA-R potentiators with lower risks of bell-shaped

response. Based on the strategy, we have discovered a clinical candidate, TAK-653, with

lower risks of both *in vitro* and *in vivo* bell-shaped response (manuscripts in preparation).

JPET#245050

Acknowledgments

JPET#245050

Authorship Contributions

Participated in research design: Kunugi, Kimura.

Conducted experiments: Kunugi, Tajima, Kuno, Sogabe

Performed data analysis: Kunugi, Tajima, Kuno, Sogabe

Wrote or contributed to the writing of the manuscript: Kunugi, Sogabe, Kimura.

42

JPET#245050

References

Armstrong N and Gouaux E (2000) Mechanisms for activation and antagonism of an

AMPA-sensitive glutamate receptor: crystal structures of the GluR2 ligand binding

core. *Neuron* **28**:165-181.

Bai F, Bergeron M and Nelson DL (2003) Chronic AMPA receptor potentiator (LY451646)

treatment increases cell proliferation in adult rat hippocampus. *Neuropharmacology*

44:1013-1021.

Balaratnasingam S and Janca A (2012) Brain Derived Neurotrophic Factor: a novel

neurotrophin involved in psychiatric and neurological disorders. *Pharmacol Ther*

134:116-124.

Beattie EC, Carroll RC, Yu X, Morishita W, Yasuda H, von Zastrow M and Malenka RC

(2000) Regulation of AMPA receptor endocytosis by a signaling mechanism shared

with LTD. *Nat Neurosci* **3**:1291-1300.

Bernard K, Danober L, Thomas JY, Lebrun C, Munoz C, Cordi A, Desos P, Lestage P and

Morain P (2010) DRUG FOCUS: S 18986: A positive allosteric modulator of

AMPA-type glutamate receptors pharmacological profile of a novel cognitive

enhancer. *CNS Neurosci Ther* **16**:e193-212.

Boulter J, Hollmann M, O'Shea-Greenfield A, Hartley M, Deneris E, Maron C and

Heinemann S (1990) Molecular cloning and functional expression of glutamate

receptor subunit genes. *Science* **249**:1033-1037.

Chen VB, Arendall WB, 3rd, Headd JJ, Keedy DA, Immormino RM, Kapral GJ, Murray LW,

Richardson JS and Richardson DC (2010) MolProbity: all-atom structure validation

for macromolecular crystallography. *Acta Crystallogr D Biol Crystallogr* **66**:12-21.

Derkach VA, Oh MC, Guire ES and Soderling TR (2007) Regulatory mechanisms of AMPA

receptors in synaptic plasticity. *Nat Rev Neurosci* **8**:101-113.

Ehlers MD (2000) Reinsertion or degradation of AMPA receptors determined by

activity-dependent endocytic sorting. *Neuron* **28**:511-525.

Emsley P, Lohkamp B, Scott WG and Cowtan K (2010) Features and development of Coot.

Acta Crystallogr D Biol Crystallogr **66**:486-501.

Fletcher EJ, Nutt SL, Hoo KH, Elliott CE, Korczak B, McWhinnie EA and Kamboj RK

(1995) Cloning, expression and pharmacological characterization of a human

glutamate receptor: hGluR4. *Receptors Channels* **3**:21-31.

Fowler JH, Whalley K, Murray T, O'Neill M J and McCulloch J (2004) The AMPA receptor

potentiator LY404187 increases cerebral glucose utilization and c-fos expression in

the rat. *J Cereb Blood Flow Metab* **24**:1098-1109.

Hardingham GE, Cruzalegui FH, Chawla S and Bading H (1998) Mechanisms controlling

gene expression by nuclear calcium signals. *Cell Calcium* **23**:131-134.

Jhee SS, Chappell AS, Zarotsky V, Moran SV, Rosenthal M, Kim E, Chalon S, Toublanc N,

Brandt J, Coutant DE and Ereshefsky L (2006) Multiple-dose plasma pharmacokinetic
and safety study of LY450108 and LY451395 (AMPA receptor potentiators) and their
concentration in cerebrospinal fluid in healthy human subjects. *J Clin Pharmacol*
46:424-432.

Kaae BH, Harpsoe K, Kastrup JS, Sanz AC, Pickering DS, Metzler B, Clausen RP, Gajhede
M, Sauerberg P, Liljefors T and Madsen U (2007) Structural proof of a dimeric
positive modulator bridging two identical AMPA receptor-binding sites. *Chem Biol*
14:1294-1303.

Kato AS, Siuda ER, Nisenbaum ES and Bredt DS (2008) AMPA receptor subunit-specific
regulation by a distinct family of type II TARPs. *Neuron* **59**:986-996.

Keinanen K, Wisden W, Sommer B, Werner P, Herb A, Verdoorn TA, Sakmann B and
Seeburg PH (1990) A family of AMPA-selective glutamate receptors. *Science*
249:556-560.

Kew JN and Kemp JA (2005) Ionotropic and metabotropic glutamate receptor structure and
pharmacology. *Psychopharmacology (Berl)* **179**:4-29.

Mackowiak M, O'Neill MJ, Hicks CA, Bleakman D and Skolnick P (2002) An AMPA
receptor potentiator modulates hippocampal expression of BDNF: an in vivo study.
Neuropharmacology **43**:1-10.

Miu P, Jarvie KR, Radhakrishnan V, Gates MR, Ogden A, Ornstein PL, Zarrinmayeh H, Ho

K, Peters D, Grabell J, Gupta A, Zimmerman DM and Bleakman D (2001) Novel

AMPA receptor potentiators LY392098 and LY404187: effects on recombinant

human AMPA receptors in vitro. *Neuropharmacology* **40**:976-983.

Murray TK, Whalley K, Robinson CS, Ward MA, Hicks CA, Lodge D, Vandergriff JL,

Baumbarger P, Siuda E, Gates M, Ogden AM, Skolnick P, Zimmerman DM,

Nisenbaum ES, Bleakman D and O'Neill MJ (2003) LY503430, a novel

alpha-amino-3-hydroxy-5-methylisoxazole-4-propionic acid receptor potentiator with

functional, neuroprotective and neurotrophic effects in rodent models of Parkinson's

disease. *J Pharmacol Exp Ther* **306**:752-762.

Murshudov GN, Skubak P, Lebedev AA, Pannu NS, Steiner RA, Nicholls RA, Winn MD,

Long F and Vagin AA (2011) REFMAC5 for the refinement of macromolecular

crystal structures. *Acta Crystallogr D Biol Crystallogr* **67**:355-367.

Nakanishi N, Shneider NA and Axel R (1990) A family of glutamate receptor genes: evidence

for the formation of heteromultimeric receptors with distinct channel properties.

Neuron **5**:569-581.

O'Neill MJ, Bleakman D, Zimmerman DM and Nisenbaum ES (2004) AMPA receptor

potentiators for the treatment of CNS disorders. *Curr Drug Targets CNS Neurol

Disord* **3**:181-194.

O'Neill MJ and Dix S (2007) AMPA receptor potentiators as cognitive enhancers. *IDrugs*

10:185-192.

O'Neill MJ and Witkin JM (2007) AMPA receptor potentiators: application for depression

and Parkinson's disease. *Curr Drug Targets* **8**:603-620.

Otwinowski Z and Minor W (1997) Processing of X-ray Diffraction Data Collected in

Oscillation Mode *Methods in Enzymology* **276**:307-326.

Patel NC, Schwarz J, Hou XJ, Hoover DJ, Xie L, Fliri AJ, Gallaschun RJ, Lazzaro JT, Bryce

DK, Hoffmann WE, Hanks AN, McGinnis D, Marr ES, Gazard JL, Hajos M, Scialis

RJ, Hurst RS, Shaffer CL, Pandit J and O'Donnell CJ (2013) Discovery and

characterization of a novel dihydroisoxazole class of

alpha-amino-3-hydroxy-5-methyl-4-isoxazolepropionic acid (AMPA) receptor

potentiators. *J Med Chem* **56**:9180-9191.

Schoft VK, Schopoff S and Jantsch MF (2007) Regulation of glutamate receptor B

pre-mRNA splicing by RNA editing. *Nucleic Acids Res* **35**:3723-3732.

Shaffer CL, Hurst RS, Scialis RJ, Osgood SM, Bryce DK, Hoffmann WE, Lazzaro JT, Hanks

AN, Lotarski S, Weber ML, Liu J, Menniti FS, Schmidt CJ and Hajos M (2013)

Positive allosteric modulation of AMPA receptors from efficacy to toxicity: the

interspecies exposure-response continuum of the novel potentiator PF-4778574. *J

Pharmacol Exp Ther* **347**:212-224.

Shieh PB and Ghosh A (1999) Molecular mechanisms underlying activity-dependent

regulation of BDNF expression. *J Neurobiol* **41**:127-134.

Sobolevsky AI, Rosconi MP and Gouaux E (2009) X-ray structure, symmetry and mechanism of an AMPA-subtype glutamate receptor. *Nature* **462**:745-756.

Sommer B, Keinanen K, Verdoorn TA, Wisden W, Burnashev N, Herb A, Kohler M, Takagi T, Sakmann B and Seeburg PH (1990) Flip and flop: a cell-specific functional switch in glutamate-operated channels of the CNS. *Science* **249**:1580-1585.

Sukumaran M, Rossmann M, Shrivastava I, Dutta A, Bahar I and Greger IH (2011) Dynamics and allosteric potential of the AMPA receptor N-terminal domain. *EMBO J* **30**:972-982.

Tao X, Finkbeiner S, Arnold DB, Shaywitz AJ and Greenberg ME (1998) Ca2+ influx regulates BDNF transcription by a CREB family transcription factor-dependent mechanism. *Neuron* **20**:709-726.

Tomita S (2010) Regulation of ionotropic glutamate receptors by their auxiliary subunits. *Physiology (Bethesda)* **25**:41-49.

Vagin A and Teplyakov A (2010) Molecular replacement with MOLREP. *Acta Crystallogr D Biol Crystallogr* **66**:22-25.

Ward SE, Bax BD and Harries M (2010) Challenges for and current status of research into positive modulators of AMPA receptors. *Br J Pharmacol* **160**:181-190.

Winn MD, Ballard CC, Cowtan KD, Dodson EJ, Emsley P, Evans PR, Keegan RM, Krissinel

EB, Leslie AG, McCoy A, McNicholas SJ, Murshudov GN, Pannu NS, Potterton EA,

Powell HR, Read RJ, Vagin A and Wilson KS (2011) Overview of the CCP4 suite and

current developments. *Acta Crystallogr D Biol Crystallogr* **67**:235-242.

Yamada KA (1998) Modulating excitatory synaptic neurotransmission: potential treatment for

neurological disease? *Neurobiol Dis* **5**:67-80.

Yelshanskaya MV, Li M and Sobolevsky AI (2014) Structure of an agonist-bound ionotropic

glutamate receptor. *Science* **345**:1070-1074.

Zarrinmayeh H, Bleakman D, Gates MR, Yu H, Zimmerman DM, Ornstein PL, McKennon T,

Arnold MB, Wheeler WJ and Skolnick P (2001)

[3H]N-2-(4-(N-benzamido)phenyl)propyl-2-propanesulfonamide: a novel AMPA

receptor potentiator and radioligand. *J Med Chem* **44**:302-304.

JPET#245050

Footnotes

This work was funded by Takeda Pharmaceutical Company Limited.

All authors are employees of Takeda Pharmaceutical Company Limited.

JPET#245050

Figure Legends

Fig. 1. LY451646 and LY451395 showed a bell-shaped response for BDNF protein

production in primary neurons in the presence of agonist. (A) Chemical structures of

LY451646 and LY451395. (B, C) Effects of LY451646 and LY451395 on BDNF protein

levels in primary neurons (B) and LDH release from primary neurons (C). Cells were treated

with LY451646 and LY451395 for 24 h in the presence (black bar) or absence (white bar) of

1 μM AMPA. Data are presented as mean ± SD, n = 3. Concentration-dependent effects of

test compounds were statistically analyzed using the one-tailed Williams' test ($^{\#}P \leq 0.025$;

versus control group). Statistical significance of differences between control and test

compounds in the BDNF assay using AMPA was determined using Dunnett's test ($^{*}P \leq 0.05$,

$^{***}P \leq 0.001$).

Fig. 2. LY451395 showed agonistic effects in primary neurons, but not in GluA1i CHO cells.

(A) Effects of LY451395 on AMPA receptor-mediated currents in the presence or absence of

1 μM AMPA in a patch-clamp study using primary neurons. Data are presented as the mean ±

SEM (n = 4-9). (B) Effects of LY451395 on Ca^{2+} influx in primary neurons in the presence or

absence of 5 μM AMPA. (C) Effects of LY451395 on Ca^{2+} influx in GluA1i CHO cells in the

presence or absence of 3 mM glutamate. (D) Effects of LY451395 and NBQX on the binding

51

of [^{3}H]-AMPA to rat hippocampal membranes. Data are presented as mean ± SD, n=3-4.

Fig. 3. HBT1 activated AMPA-R in an agonist-dependent manner and increased BDNF

protein levels at a broader range of concentrations in primary neurons compared to LY451395

and OXP1 (A) Chemical structure of HBT1 and OXP1. (B, C) Effects of HBT1 (B) and

OXP1 (C) on Ca^{2+} influx in GluAi CHO cells in the presence or absence of 3 mM glutamate.

(D) Effects of 100 μM NBQX on the induction of Ca^{2+} influx by HBT1 or OXP1 in the

presence of 10 μM glutamate. (E, F) Effects of HBT1 (E) and OXP1 (F) on Ca^{2+} influx in

primary neurons in the presence or absence of 5 μM AMPA. (G) Effects of 10 μM NBQX on

the induction of Ca^{2+} influx by 10 μM HBT1 or 10 μM OXP1 in the presence of 5 μM AMPA.

(H) Effects of HBT1 and OXP1 on AMPA receptor-mediated currents in the presence or

absence of 1 μM AMPA in a patch-clamp study using primary neurons. Data are presented as

the mean ± SEM (n = 4-9). (I, J) Effects of HBT1 and OXP1 on BDNF protein levels in

primary neurons (I) and LDH release from primary neurons (J). Cells were treated with HBT1

or OXP1 for 24 h in the presence (black bar) or absence (white bar) of AMPA (1 μM). Data

are presented as mean ± SD, n = 3. Concentration-dependent effects of test compounds were

statistically analyzed using the one-tailed Williams' test ([#]P ≤ 0.025; versus control group).

Statistical significance of differences between control and OXP1 in the BDNF assay using

AMPA was determined using Dunnett's test ([**]P ≤ 0.01, [***]P ≤ 0.001). (K) Concentration of

glutamate required for the induction of Ca^{2+} influx by 30 μM HBT1 and 30 μM OXP1 in

GluA1i CHO cells. Other data (B-G and K) are presented as mean ± SD, n = 3. The statistical

significance of differences between NBQX (-) and NBQX (+) in (D) and (G) was determined

using Aspin-Welch's *t*-test or Student's *t*-test ([***]P ≤ 0.001).

Fig. 4. HBT1 and LY451395 bound to a pocket in the LBD of AMPA-R using a different

binding mode. (A) SPA measurement of selective [3H]-HBT1 binding to His-tagged GluA2o

LBD (His-LBD). The 6His-tagged human MIF (His-MIF) was used as a control protein. (B)

SPA measurement of selective [3H]-OXP1 binding to His-LBD. (C) Effects of glutamate on

the binding of [3H]-HBT1 to His-LBD. (D) Analysis of saturation isotherms with [3H]-HBT1

indicating a single saturable binding site in His-LBD. (E) Displacement studies with HBT1

and LY451395 using SPA with [3H]-HBT1 and His-LBD. (F) Effects of glutamate on the

binding of [3H]-HBT1 to hippocampal membranes. (G) Analysis of saturation isotherms with

[3H]-HBT1 disclosing a single saturable binding site in rat hippocampal membranes. (H)

Displacement studies with HBT1 and LY451395 using the binding assay with [3H]-HBT1 and

rat hippocampal membranes. (I) Overall structure of GluA2o LBD in complex with HBT1

and LY451395. HBT1 and LY451395 are shown in yellow, glutamate is shown in gray, and

the two protomers comprising the dimer are shown in green (protomer A) and cyan (protomer

B). Both compounds bind at the dimer interface in two symmetrical orientations. It is noted

that only one of the conformations is described, for clarity. (J) Close-up view of the binding

site of HBT1 (upper) and LY451395 (lower). The compounds are shown in yellow. The

protomers A and B are shown in green and cyan, respectively. The side chains of S518 and

S750 exhibit alternative conformations. Hydrogen bonds are shown as orange dashed lines.

Data are presented as mean ± SD, n = 3–4. Concentration-dependent effects of His-LBD in

(A) and (B) were statistically analyzed using the one-tailed Williams' test ($^{\#}P \leq 0.025$; versus

control group).

Fig. 5. OXP1, via binding to a different site from that of HBT1, promoted binding between

HBT1 and AMPA-R and activated AMPA-R in the absence of agonist. (A, B) Effects of

OXP1 on [³H]-HBT1 binding to His-LBD (A) and rat hippocampal membranes (B). (C) SPA

measurement of selective [³H]-OXP1 binding to His-tagged GluA2o ATD (His-ATD).

His-MIF was used as control protein. (D) Effects of glutamate on the binding of [³H]-OXP1

to His-ATD. (E, F) Effects of co-application of HBT1 and OXP1 on Ca^{2+} influx in the

absence of agonist in primary neurons (E) or GluA1i CHO cells (F). (G) Effects of 10 μM

NBQX on the induction of Ca^{2+} influx by co-application of HBT1 and 10 μM OXP1 in the

absence of AMPA. (H) Effects of OXP1 on the binding of [³H]-HBT1 to hippocampal

membranes in the absence of glutamate or at 30 μM glutamate. Data are presented as mean ±

SD, n = 3–4. Concentration-dependent effects of His-ATD (C) or test compounds (H) were

statistically analyzed using the one-tailed Williams' test ($^{\#}P \leq 0.025$; versus control group).
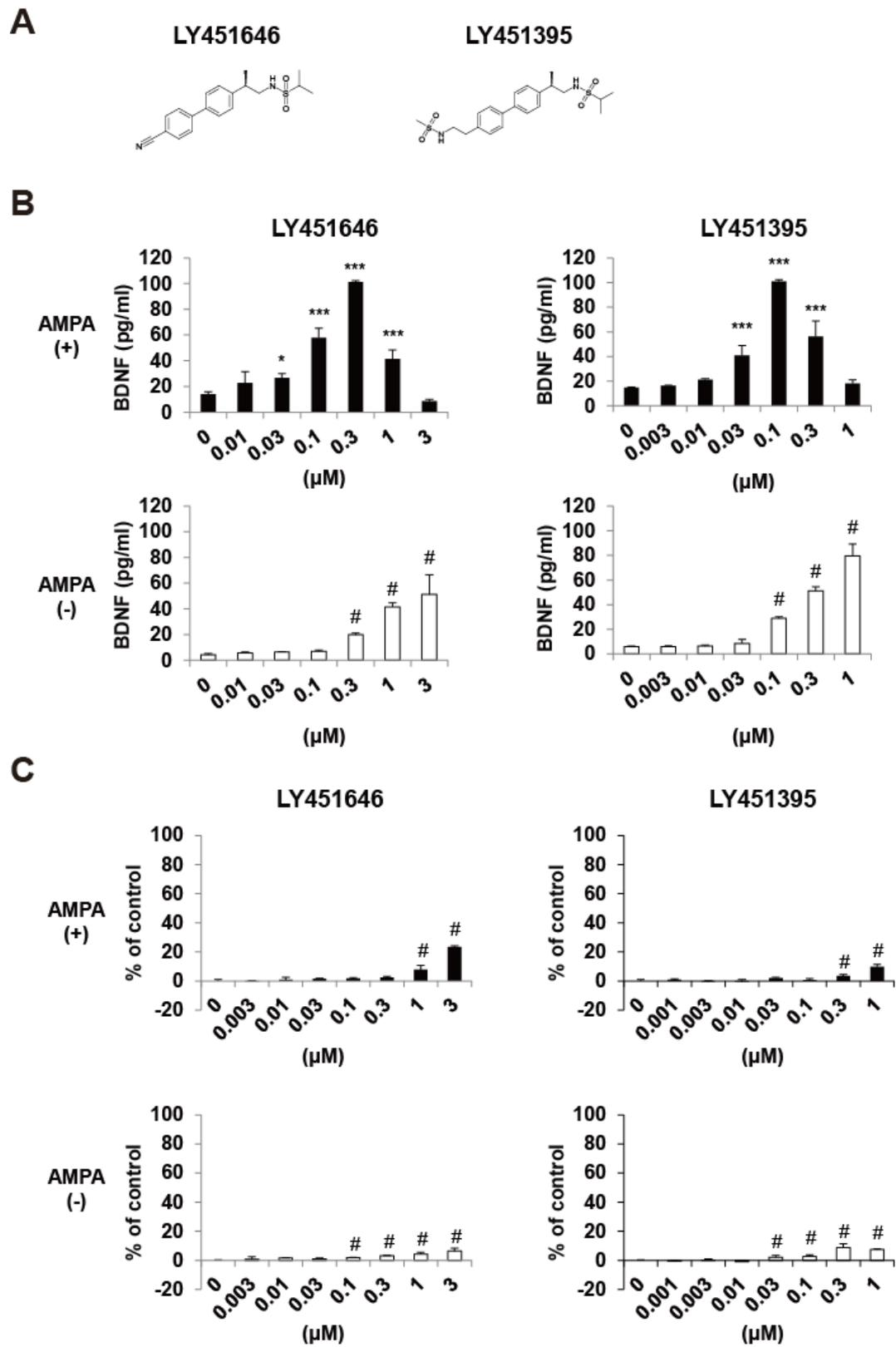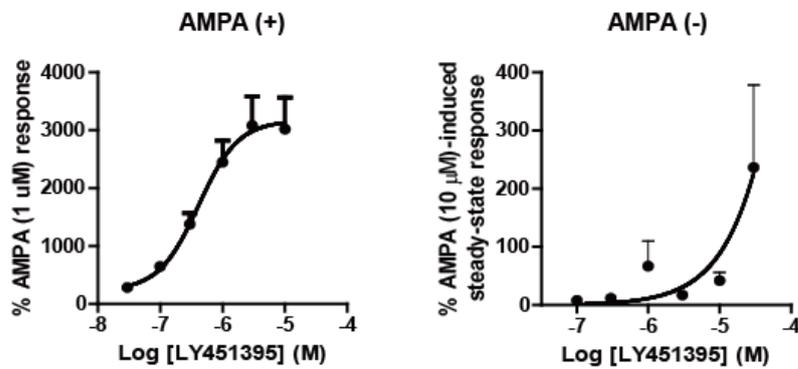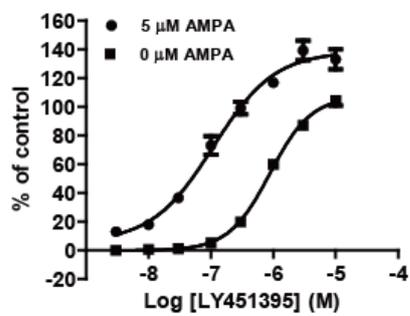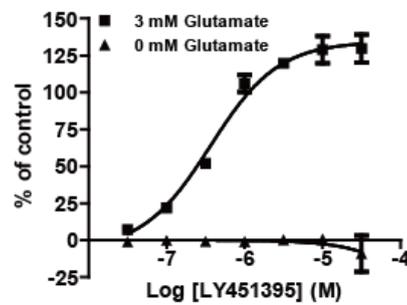
Fig. 1

Fig. 2

Fig. 3

Fig. 4

Fig. 5